ARMY RESEARCH LABORATORY

Investigations Into Alternate Spark Gap Switching Techniques

Brian G. Smith

ARL-TR-623

September 1994

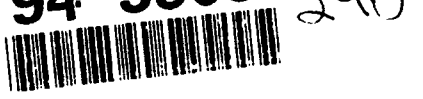

LabVIEW® is a registered trademark of National Instruments Corporation.

Tektronix® is a registered trademark of Tektronix, Inc.

The findings in this report are not to be construed as an official Department of the Army position unless so designated by other authorized documents.

Citation of manufacturer's or trade names does not constitute an official endorsement or approval of the use thereof.

Destroy this report when it is no longer needed. Do not return it to the originator.

REPORT DOCUMENTATION PAGE

Form Approved
OMB No. 0704-0188

1. AGENCY USE ONLY (Leave blank)	2. REPORT DATE	3. REPORT TYPE AND DATES COVERED
	September 1994	Final

4. TITLE AND SUBTITLE

Investigations Into Alternate Spark Gap Switching Techniques

5. FUNDING NUMBERS

PR: 4XE9X1
PE: P612120H25

6. AUTHOR(S)

Smith, B. G.

7. PERFORMING ORGANIZATION NAME(S) AND ADDRESS(ES)

U.S. Army Research Laboratory
Survivability & Lethality Directorate
Aberdeen Proving Ground, MD 21010-5423

8. PERFORMING ORGANIZATION REPORT NUMBER

9. SPONSORING/MONITORING AGENCY NAME(S) AND ADDRESS(ES)

U.S. Army Research Laboratory
Survivability & Lethality Directorate
Aberdeen Proving Ground, MD 21010-5423

10. SPONSORING/MONITORING AGENCY REPORT NUMBER

ARL-TR-623

11. SUPPLEMENTARY NOTES

12a. DISTRIBUTION/AVAILABILITY STATEMENT

Approved for public release; distribution is unlimited.

12b. DISTRIBUTION CODE

13. ABSTRACT (Maximum 200 words)

This report documents the design, operation, and experimental results of the evaluation of a new spark gap triggering method. These spark gaps were developed to support ARL's ongoing nuclear electromagnetic pulse (EMP) current injection assessment programs. This trigger method provides operator control, multiple spark gap control with synchronous triggering, and a limited amount of hardware to control the spark gap triggering. A patent application has been started for this device and has been assigned case number HDL No. 94-3.

14. SUBJECT TERMS

current injection
spark gap

15. NUMBER OF PAGES

20

16. PRICE CODE

17. SECURITY CLASSIFICATION OF REPORT	18. SECURITY CLASSIFICATION OF THIS PAGE	19. SECURITY CLASSIFICATION OF ABSTRACT	20. LIMITATION OF ABSTRACT
Unclassified	Unclassified	Unclassified	

INTENTIONALLY LEFT BLANK.

TABLE OF CONTENTS

INTENTIONALLY LEFT BLANK.

LIST OF FIGURES

INTENTIONALLY LEFT BLANK.

INVESTIGATIONS INTO ALTERNATE SPARK GAP SWITCHING TECHNIQUES

1. INTRODUCTION

This report documents the experimental design and findings determined in the evaluation of a new spark gap triggering method. This spark gap design was developed and tested on a part-time basis at the U.S. Army Research Laboratory (ARL) Woodbridge Research Facility (WRF) in fiscal years (FY) 93 and 94. The design was driven by the need to improve in-house and commercially available spark gaps for a new current injector design. The anticipated benefits of this new approach are operator-controlled triggering, multiple spark gap synchronous triggering, a high number of spark gaps controlled simultaneously, and a limited amount of hardware to control the triggering.

2. BACKGROUND

This spark gap triggering methodology was developed in the process of designing a current injection device capable of reproducing the short commercial power line threat for MIL-STD-188-125. MIL-STD-188-125 provides design guidelines and assessment procedures to ensure that C4I systems are survivable against nuclear high altitude electromagnetic pulse (HEMP). Current injection is used to assess the performance of power line protection devices. MIL-STD-188-125 requires a fast rise time, short duration waveform to simulate the worst case HEMP coupling for the three-phase commercial power line grid. The standard requires a differential mode peak current of 4 kA per phase and a common mode peak current of 8 kA per phase. Interpreting the MIL-STD's requirements resulted in a current injector capable of firing a single output at 4 kA and firing four outputs (three phases + neutral) at 2 kA for a total common mode amplitude of 8 kA. The working group for MIL-STD-188-125 defined the source impedance for the current injector as 67 ohms (Ω). Using the 4-kA-per-phase peak current results in a minimum output level of 270 kV. Design optimization led to a four-stage Marx configuration requiring four triggerable spark gaps to separate the capacitors.

During the design of the MIL-STD-188-125 pulser, two triggering requirements became clear: (1) The trigger mechanism must be capable of simultaneously triggering 16 spark gaps, and (2) the space typically used in trigger circuits was unavailable because of other design requirements. Standard commercial or in-house trigger methods were unable to meet these requirements.

3. SPARK GAP CONSTRUCTION

Two spark gaps were built at the ARL WRF machine shop to be used for the operational checkout and experimentation. The gaps were built using existing spare parts when possible to minimize expenses; therefore, the two spark gaps were not identical. All critical dimensions were, however, maintained to within ±0.003 inch for the two gaps. Figure 1 shows the general construction of the gaps, and the critical dimensions are labeled. The end plates of the gaps were machined from aluminum, and the main and output electrodes were machined from brass. The dielectric switch housing was constructed from Plexiglas with an O-ring groove machined at each end to seal with the end plates. Nylon bolts are used to secure the end plates and the switch housing together as a unit. The internal portion of the spark gap is pressurized with the inert gas sulfurhexafluoride (SF_6). Items not shown in Figure 1 are gas fittings for the SF_6 and mechanical fasteners for the electrodes and end plates. During this experiment, internal gas pressures ranged from 0 to 40 lb/in^2. The center electrode was constructed from the center core of a RG-58 co-ax cable. The center core provided the internal conductor already set into a flexible dielectric material. The main electrode was drilled at a sufficient diameter to provide a snug fit for the center electrode and dielectric material. No external fastening was required to hold the center electrode in place even with the electrode tip experiencing 40 lb/in^2 internal gas pressure. The surface area of the electrode end was only 0.05 in^2; hence, the center electrode only experienced 2.0-lb force from the gas pressure.

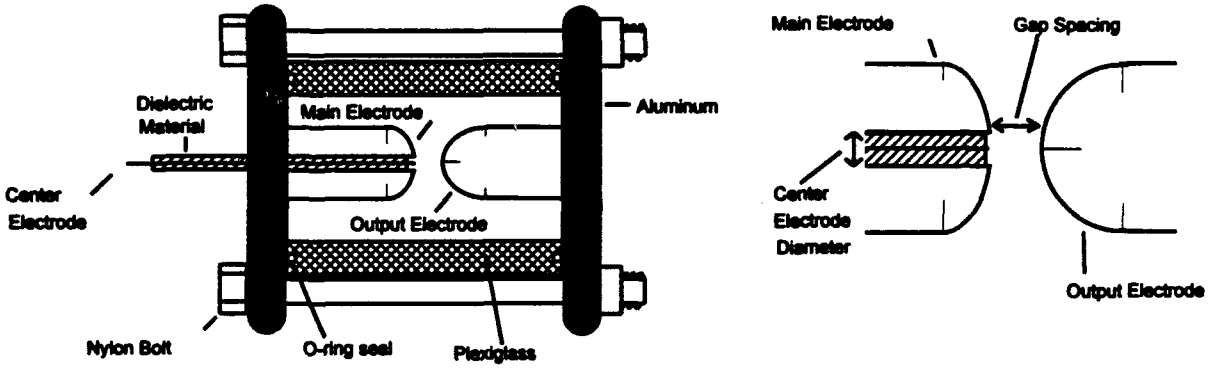

Figure 1. General construction of spark gap.

4. PRINCIPLE OF OPERATION

High voltage spark gaps are used to control the discharge of capacitors for current injection or pulse power applications. Presently, spark gaps are triggered (activated) by two methods. The first method is self breakdown whereby the voltage across the spark gap exceeds the dielectric

strength of the gas between the electrodes, and the spark gap activates itself. The self breakdown method is crude and sporadic. The breakdown level can be affected by many factors such as charge rate, dirty electrodes, contaminated dielectric gases, and attachment points on the electrodes from previous firings. Personnel operating the spark gap have very little control when the spark gap activates, and it is impossible to simultaneously trigger several spark gaps.

The second method to trigger a spark gap is to introduce a high voltage transient into the spark gap. The high voltage transient causes an initial arc inside the spark gap, thus causing the spark gap to activate. This method allows for operator control; however, the problems associated with this method are complicated triggering circuits and the inability to typically trigger more than four gaps. The typical trigger circuits involve at least two power supplies and three sequential transient generators.

This proposed triggering method has several advantages when compared to the two previous methods discussed. The switching of the spark gap is operator controlled. The control mechanism is very simple and compact compared to typical trigger circuitry. Multiple spark gaps can be operated and switched simultaneously by one control mechanism. The number of spark gaps is limited by the control mechanism, not the design of the spark gap. Commercially available components have the electrical current handling capabilities to trigger at least 20 spark gaps. The spark gap control circuits have a very high impedance; thus, they have very little influence on the capacitor discharge waveform. The high control impedance also allows the spark gaps to be stacked in series as in a Marx generator configuration. The high impedance allows for sufficient isolation between the Marx stages to prevent the trigger circuits from degrading the Marx output. The trigger components are also switched to ground when the Marx is fired so the components do not experience the elevated voltages from the Marx generator.

Figure 2 shows a single stage output spark gap in an inactive state with the high voltage relay open. The relay switch has very little contact capacitance, so the trigger resisters remain effectively at an equal potential during the capacitor charging period. There is no current flow through the center electrode or the spark gap.

Figure 3 shows the spark gap just when the high voltage relay is closed. The 2-MΩ and 200-KΩ resistors now have a voltage potential across them, and the current begins to flow from the charged capacitor through the resistors and relay switch to ground. Since the 2-MΩ resistor is much larger than the 200-KΩ resistor, most of the voltage drop appears across the 2-MΩ resistor. The center electrode, connected to the base of the 2-MΩ resistor, drops to the lower potential. The

potential between the main electrode and the center electrode is now great enough to cause an electrical arc between the main and center electrodes. At a 10-kV charge level for the capacitor, the trigger arc current is 50 milliamperes. The dielectric material between the center electrode and the main electrode causes the arc to occur at the tip of the electrodes.

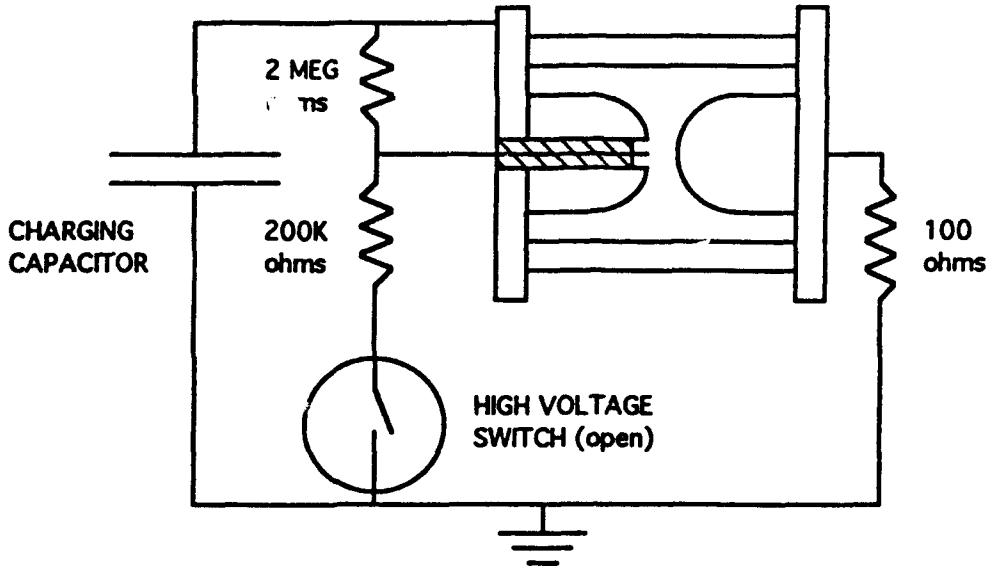

Figure 2. Spark gap in inactive stage.

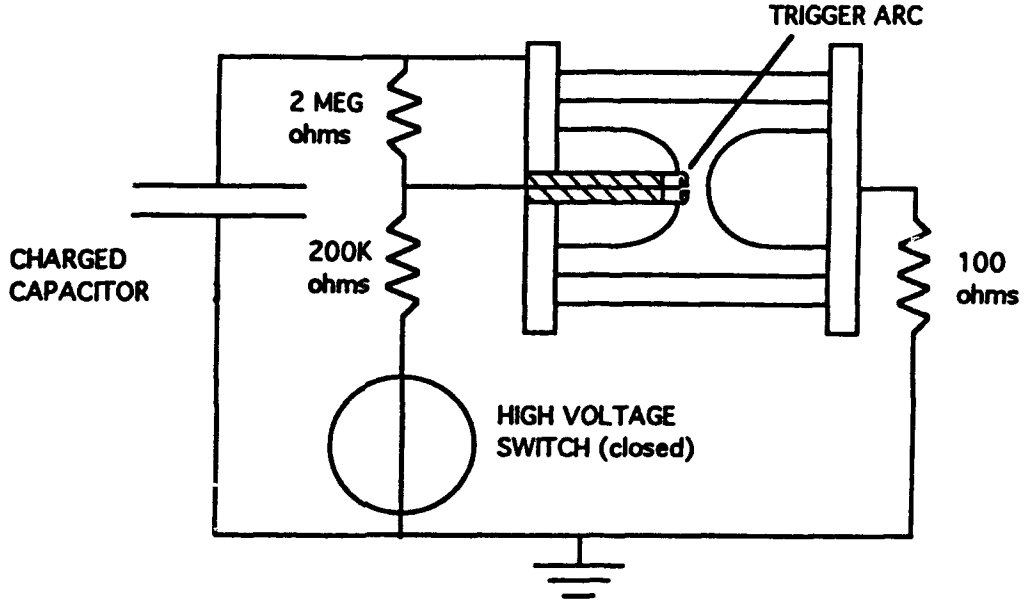

Figure 3. High voltage relay closing.

Figure 4 shows the spark gap in its activated state. The small arc from the trigger electrode caused a flow of electrons to occur inside the gap. Just as the electrons are attracted to the higher potential of the center electrode, they are attracted to the higher potential of the output electrode. The flow of electrons to the output electrode causes an ionized path to occur, and the spark gap becomes activated. Typical output resistance can range from 1 to 1000 Ω. In this particular example, the output resistance has been set to 100 Ω, and the output current would have a peak value of 100 amps. The trigger current was 50 mA and therefore has a negligible effect on the output current.

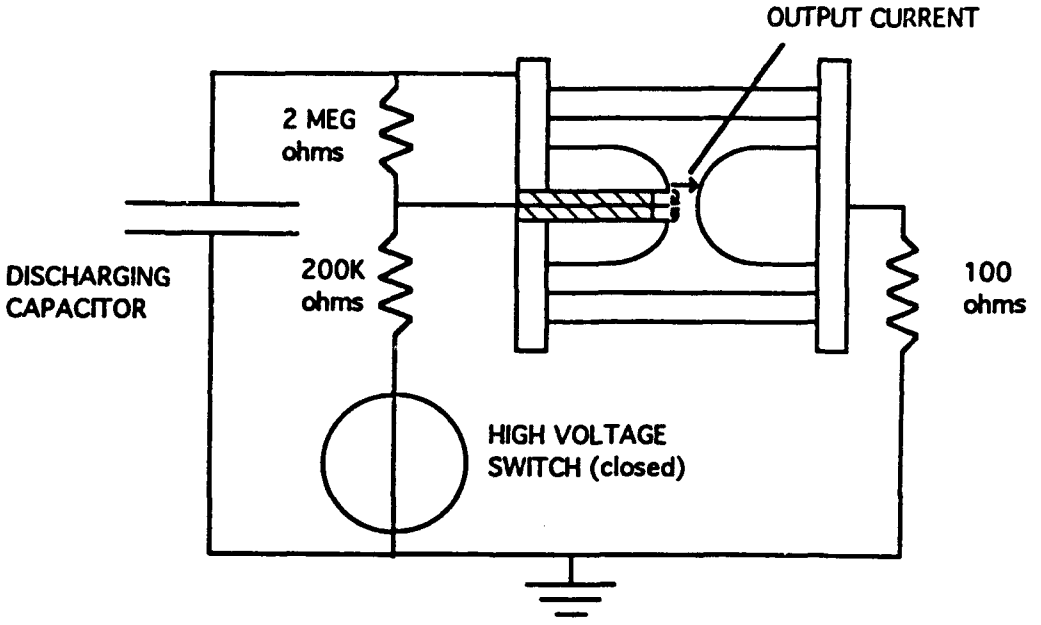

Figure 4. Activated spark gap.

5. TEST CONFIGURATIONS

Two test configurations were set up to demonstrate the capabilities of the spark gap. For both setups, the power supply was set to 10 kV. The power supply is adjustable from 0 to 40 kV, but above 16 kV, corona became a problem. The first test configuration is shown in Figure 5. A two-stage Marx generator was constructed to use the spark gaps in a series configuration and to demonstrate the ability to "stack" the spark gaps for a multistage Marx. The output current and trigger current were monitored to ensure that the spark gaps were operating as anticipated. The second test configuration (see Figure 6) used the two spark gaps in a parallel setup. The output current was

measured for each spark gap, and a differential voltage measurement was made to determine the synchronization of the two spark gaps.

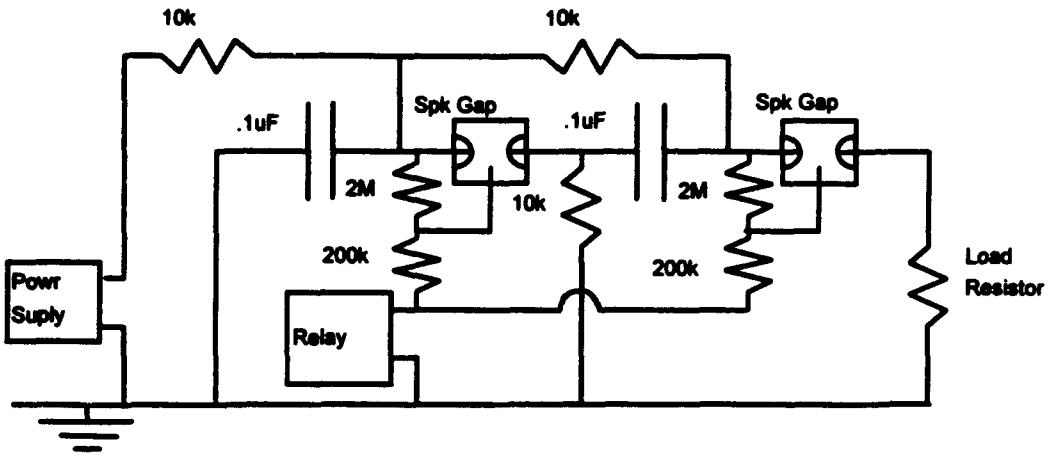

Figure 5. Marx generator test configuration.

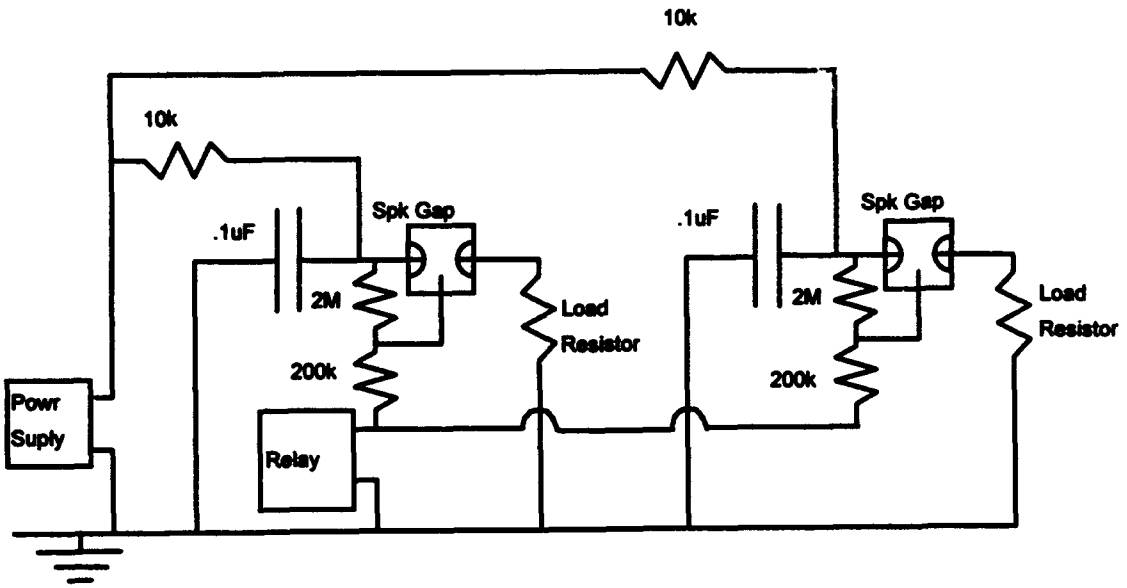

Figure 6. Parallel output test configuration.

6. TEST RESULTS

Unfortunately, the test results about to be presented are rather uninteresting. As hoped, the new spark gaps behave as any other type of triggerable spark gap. The results simply show the firing of the spark gap and the discharge of the charged capacitors. The first series of data shows the two-stage Marx generator configuration. The charge level was 10 kV per stage, and the output

resistance was 20 Ω. When the Marx generator was triggered, a peak output voltage of 20 kV was developed. Figures 7, 8, and 9 show the current through the 20-Ω output resistor. The late time data are presented to show the complete double exponential waveform. The relatively slow rise time, 10% to 90% @ 275 ns, is attributable primarily to the low output resistor value and the high dI/dt, 3.3E9 amperes/second (A/sec), causing a high inductive impedance during the rise time of the pulse. Figure 10 shows the output current when loaded with a 200-Ω resistor. The 10% to 90% rise time decreases to 75 ns, and the dI/dt decreases to 1.1E9 A/sec.

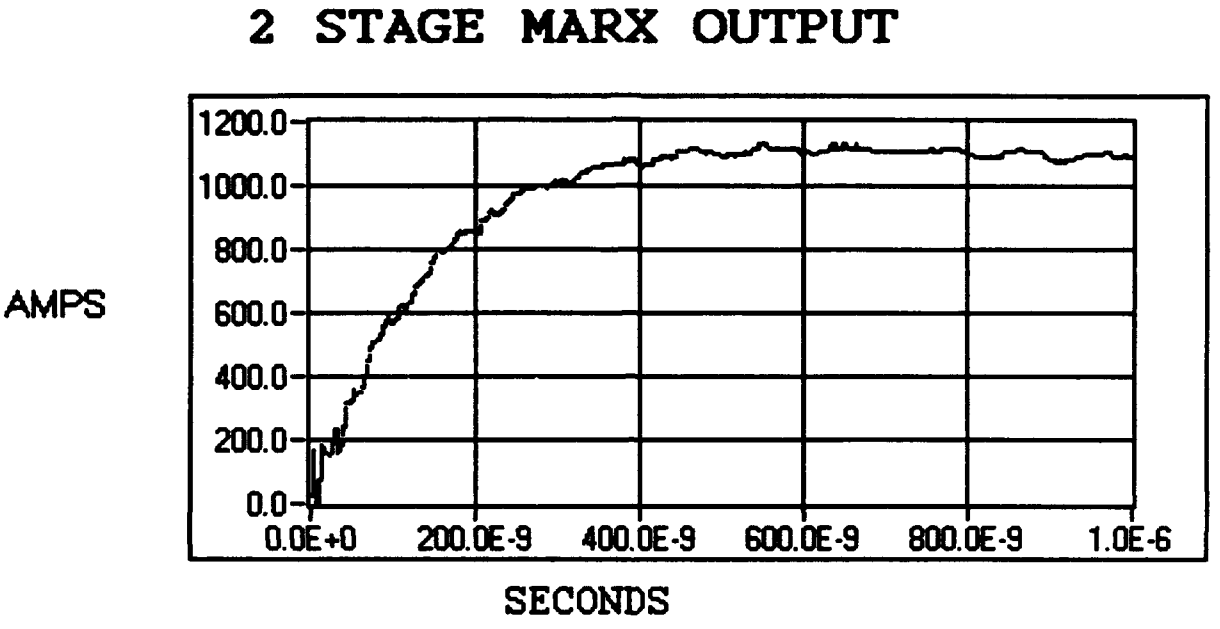

Figure 7. Marx output into 20 Ω 100 ns/division sweep.

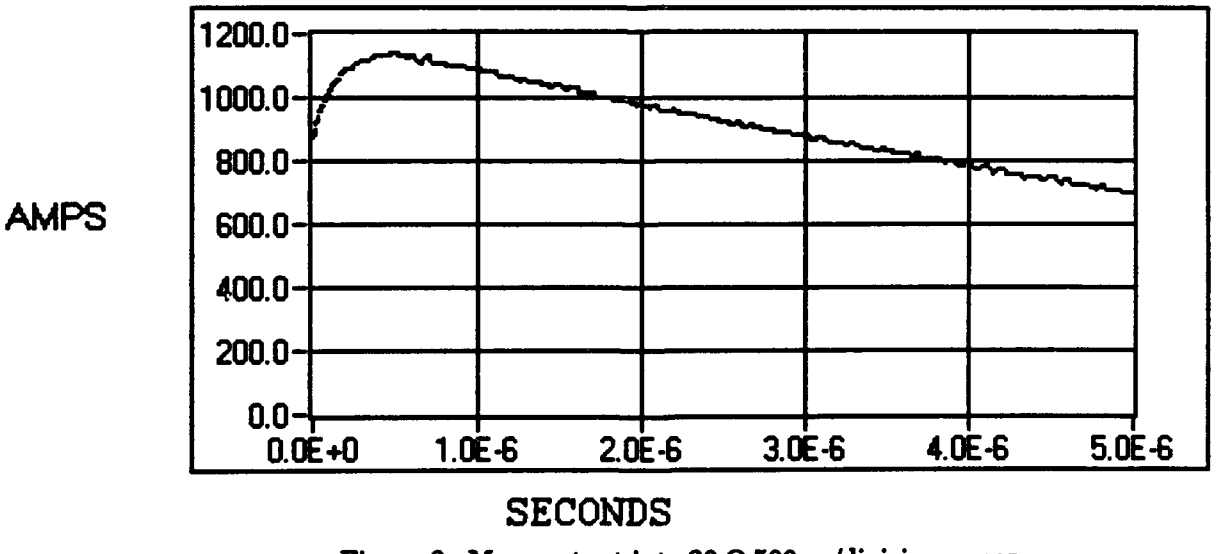

Figure 8. Marx output into 20 Ω 500 ns/division sweep.

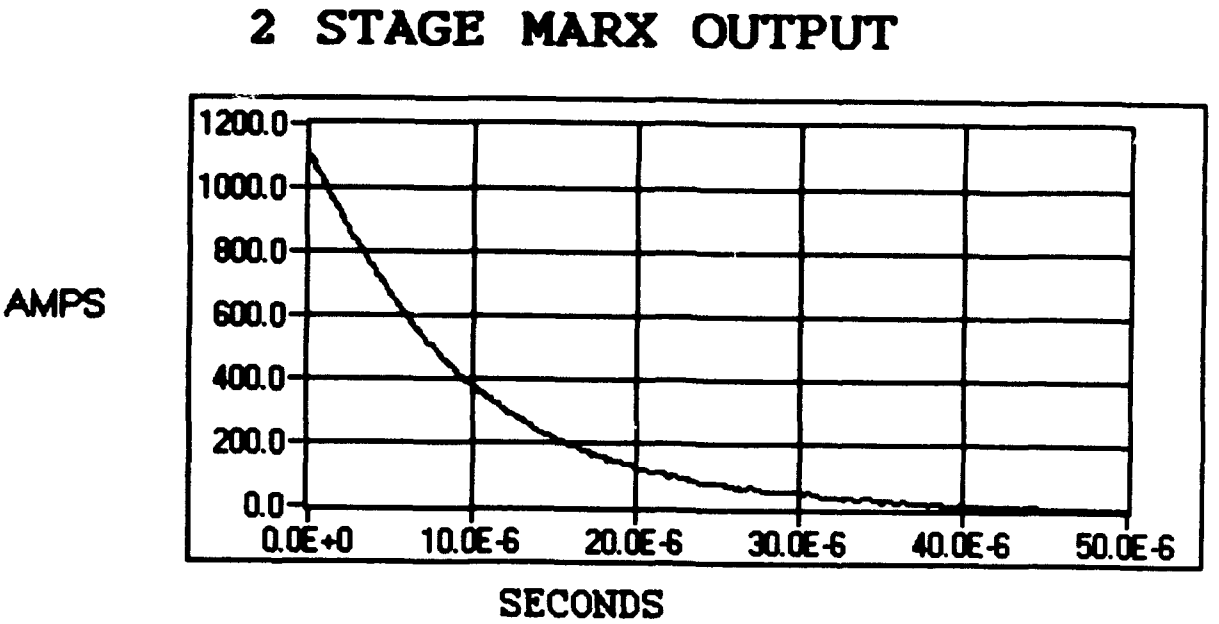

Figure 9. Marx output into 20 Ω 5 ns/division sweep.

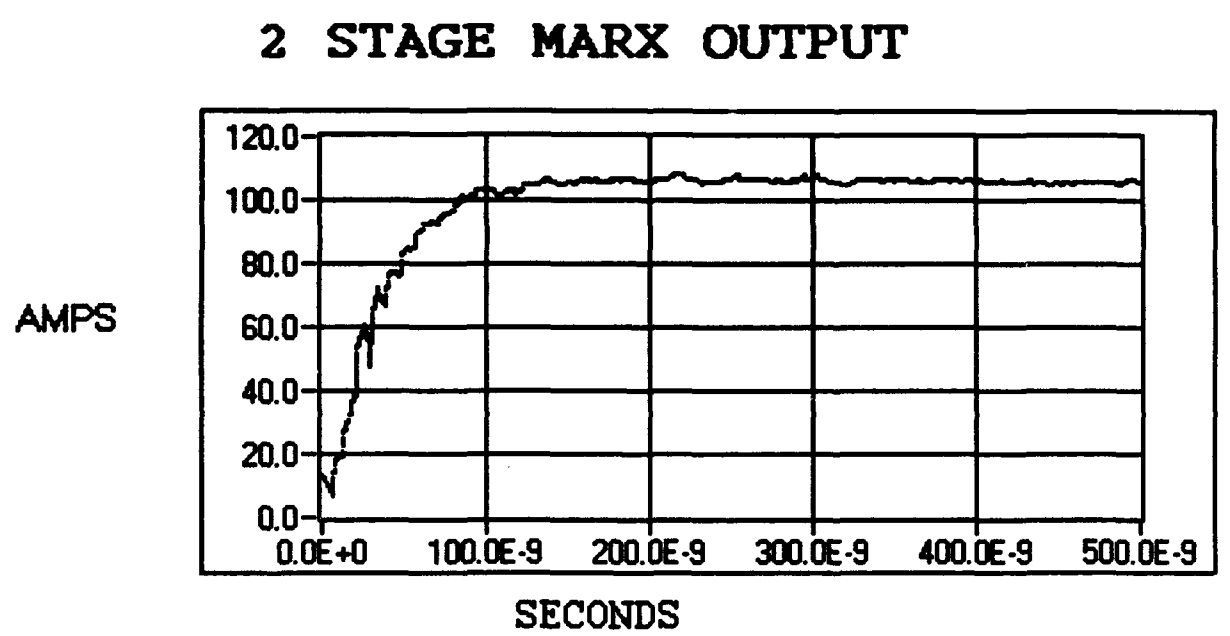

Figure 10. Marx output into 200 Ω 50 ns/division sweep.

The second test configuration was triggering two parallel output capacitors. The output was measured in two different loads as shown in Figures 11 and 12. Figure 11 is the output current

from a 10-kV charge level through a 200-Ω resistor. The 10% to 90% rise time of the pulse is 75 ns. Figure 12 is the output current from a 10-kV charge level and a 10-Ω resistor. With a higher dI/dt (2.6E9 A/sec versus 5.6E8 A/sec), the rise time increased to 325 ns.

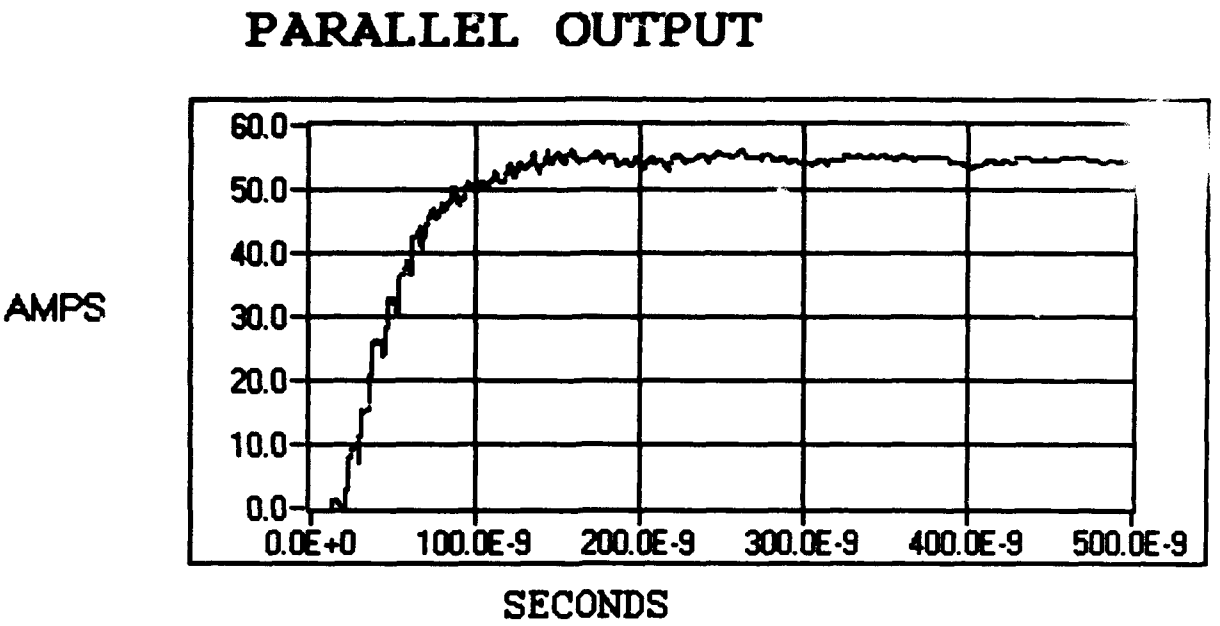

Figure 11. Parallel output into 200 Ω 50 ns/division sweep.

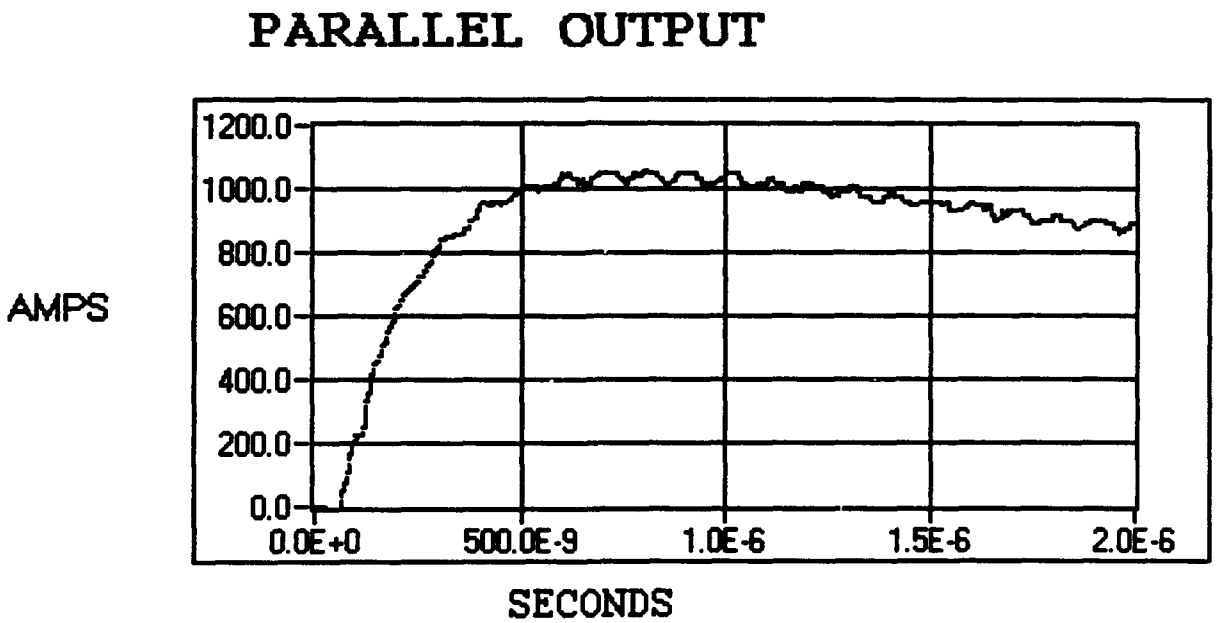

Figure 12. Parallel output into 10 Ω 200 ns/division sweep.

The second measurement made for the parallel configuration was a differential voltage measurement across the two outputs. If the spark gaps trigger simultaneously as hoped, there should not be a differential voltage to measure. Figure 13 shows the differential voltage measured. The peak amplitude was 200 V occurring in the first 20 ns. When compared to the charge level of 10 kV, the differential measurements demonstrate that the spark gaps are triggering nearly simultaneously.

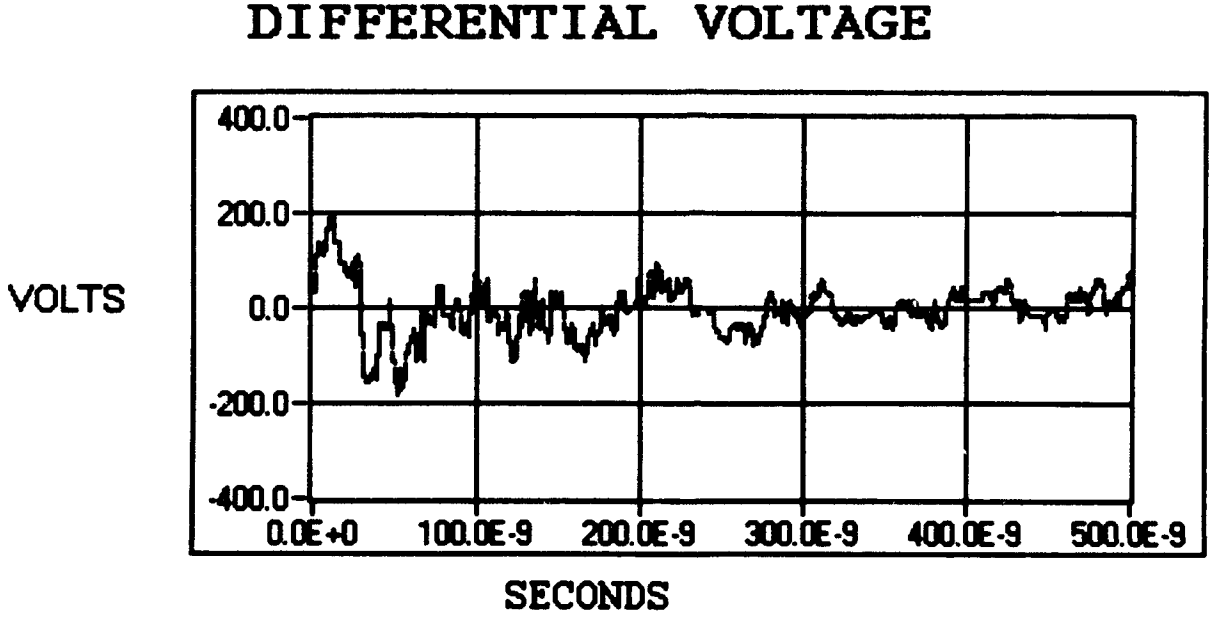

Figure 13. Differential voltage, parallel configuration.

The rise time of the low amplitude pulses contains a large amount of noise riding on the waveform. Measuring the noise peaks results in a ring frequency of 125 MHz. A significant effort was put forth to determine the cause and eliminate the noise. The instrumentation could not be triggered at any vertical setting while a "noise shot" was performed, so the noise coupling did not seem to be caused by radiated emissions. Modifications of the test fixture proved unsuccessful in determining the noise source. By changing various lead lengths on the trigger and output circuits, the author hoped to discover a shift in the ring frequency, thus identifying the noise source. Series resistance was also added between the two capacitors to eliminate the possibility of under-dampened ringing occurring between the two capacitors (in the Marx configuration) once the spark gaps were triggered. Unfortunately, none of these tactics worked either separately or together. The noise appears to be of a consistent amplitude, regardless of the output current; thus, it was more evident for the lower amplitude waveforms. In retrospect, the only common factor that was not changed was the actual trigger resistor network. An attempt was made to measure the current through the trigger resistor network. The expected peak current was 150 mA, and the

waveshape should resemble the output waveshape (i.e., a double exponential pulse). The only data collected for the trigger current were dampened sinusoids. Since no rational explanation could be made for the suspect data, the data were deemed invalid and unfit to present.

This spark gap design offers a wide variance in the operating voltage. At a specific gas pressure, the voltage could be adjusted by a factor of ~3 between the minimum voltage trigger level and the maximum voltage hold-off level. By adjusting the spark gap gas pressure between 0 and 40 lb/in^2, one can vary the spark gap's triggering levels by a factor of ~8.5 while making no mechanical changes. Figure 14 compares the maximum voltage holdoff at various gap pressures for two gap separations. Figure 15 presents the available data for the 0.065-inch gap capabilities. The charge level could not be increased beyond 16 kV while operating the test fixture in open air because of corona problems. Figure 16 documents the 0.045-inch spark gap's flexibility in triggering levels at various charge levels and gas pressures. A 40-lb/in^2 gas pressure should not be considered an unreasonably high operating pressure. Many gaps used in the labs operate at 60 lb/in^2 or higher. Unfortunately, as Figure 14 shows, increasing the gas pressure does not increase the hold-off voltage in a linear relationship. Hence, increasing the gas pressure from 40 to 60 lb/in^2 does not increase the hold-off voltage by 50%.

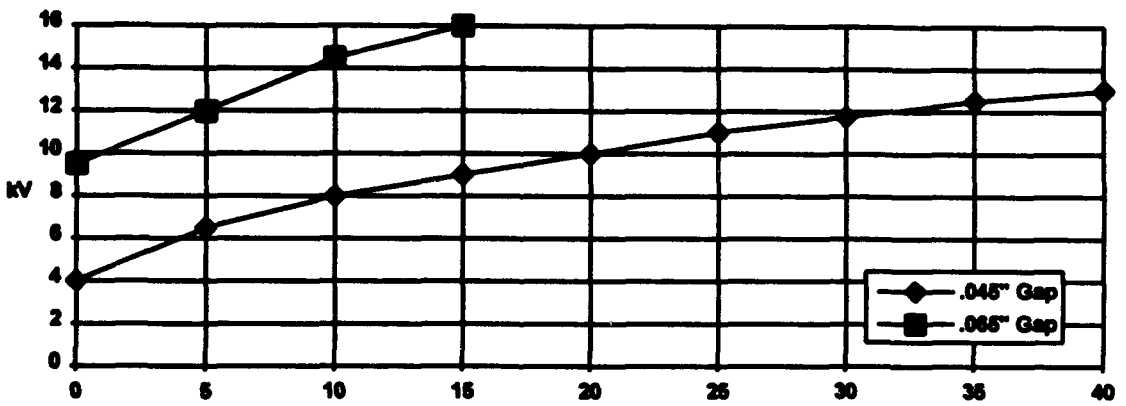

Figure 14. Voltage holdoff of two gap spacings.

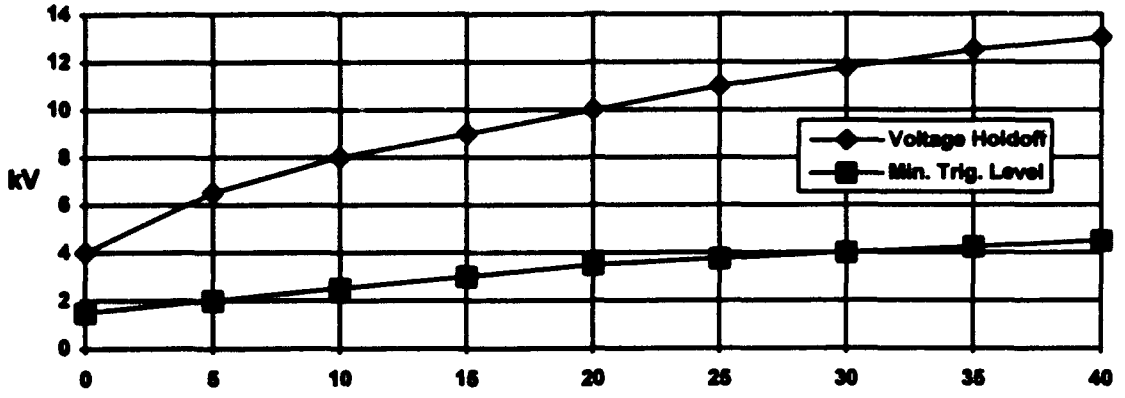

Figure 15. Gap operating range of 0.045 inch.

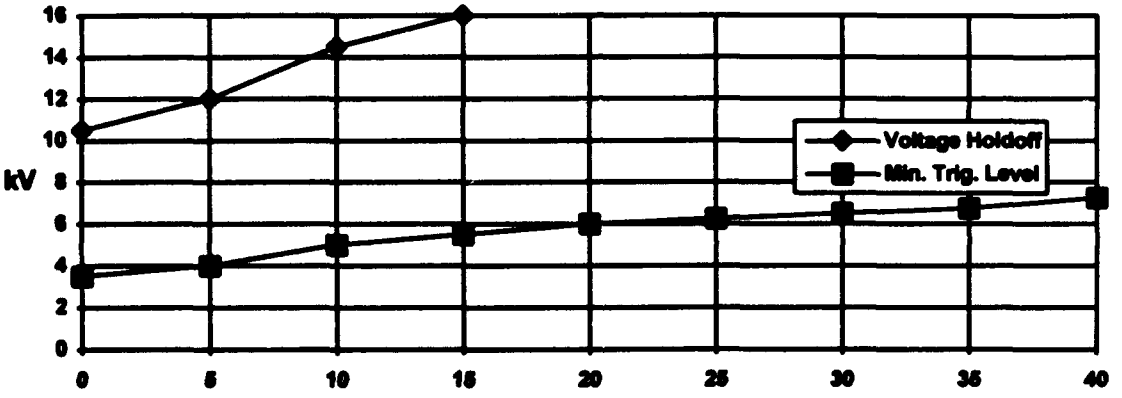

Figure 16. Gap operating range of 0.065 inch.

7. LESSONS LEARNED

During the process of testing the two configurations, several noteworthy performance characteristics were observed. There was a significant difference in the performance of the center electrode material. The center electrodes were constructed from the center conductor of two different samples of RG-58 size co-ax cables, Plastoid Corp. #77314 and Pasternack Enterprises #RG58B/U. During the testing, the Plastoid Corp. center electrode suffered severe erosion of the dielectric material around the tip. The trigger arc caused the dielectric material to melt and burn. As the spark gap firings continued, the eroded center electrode began to cause sporadic spark gap triggering. The burned material caused dirt to accumulate inside the gap and lowered the voltage hold-off level of the gap. The eroded electrode also caused the trigger arc to occur inside the main

electrode rather than at the tip. This limited the voltage triggering range by increasing the minimal voltage for a consistent spark gap firing. This phenomenon only occurred for the one electrode sample. The Pasternack Enterprises' sample was unaffected by the triggering arc.[1] At the exposed tip, some carbon paths formed from the arcing, but there was no physical degradation of the dielectric material. Once the degraded center electrode was replaced with the Pasternack Enterprises brand material, the spark gap functioned properly.

During the operational testing of the spark gaps, the maximum and minimum trigger levels were measured. If the voltage level was dropped below a certain minimum (which depended on gap spacing and gas pressure), the spark gap would not function. Once several unsuccessful attempts at very low level triggering were made, the spark gap had to be "cleared" to operate at previously attainable low trigger levels. An example of this "clearing" process is documented for a 0.045-inch gap at 15 lb/in^2. This gap could reliably hold off 9.5 kV and still operate as low as 3.5 kV with repeatable results. The spark gap failed to operate reliably at 3.0 kV. Once several unsuccessful attempts at 3.0 kV were made, the spark gap would no longer function below 5.0 kV. This phenomenon was repeatable and occurred at the same voltage levels each time. The spark gap had to be triggered several times at 6 kV before it would operate at 3.5 kV again.

8. CONCLUSION

The data presented show that this spark gap functioned similar to other types of spark gaps. This spark gap also has significant improvements over other triggerable spark gaps by reducing the complexity of the triggor circuits and increasing the number of spark gaps controlled by a single trigger circuit. The new trigger circuits will also increase reliability and reduce troubleshooting efforts. The number of components have been reduced by at least a factor of three, and all the components can be verified with a standard multimeter.

Future studies and experimentation should increase the number of spark gaps simultaneously controlled, and further investigation is needed to determine the unidentified noise source.

---

[1]The use of these co-ax cable center conductors is clearly outside their intended use. This particular comparison should not be used to judge their relative performance when they are used in applications for which they were intended.

INTENTIONALLY LEFT BLANK.

APPENDIX

DATA COLLECTION SYSTEM

INTENTIONALLY LEFT BLANK.

The test data were collected on a newly developed instrumentation control software code. LabVIEW for Windows, a National Instruments product, was used to develop an IEEE bus, GPIB format instrument driver for the Tektronix 7912 AD transient digitizer (see Figure A-1). A Gateway2000 486, 50 MHz PC with 24 MBytes RAM served as the operating system with a National Instruments AT-GPIB card providing the interface to the digitizer. Current measurements were made either with a Eaton 83363-4M or a Singer 91197-1 probe. The differential voltage measurements were performed by a Tektronix P6046 differential voltage probe.

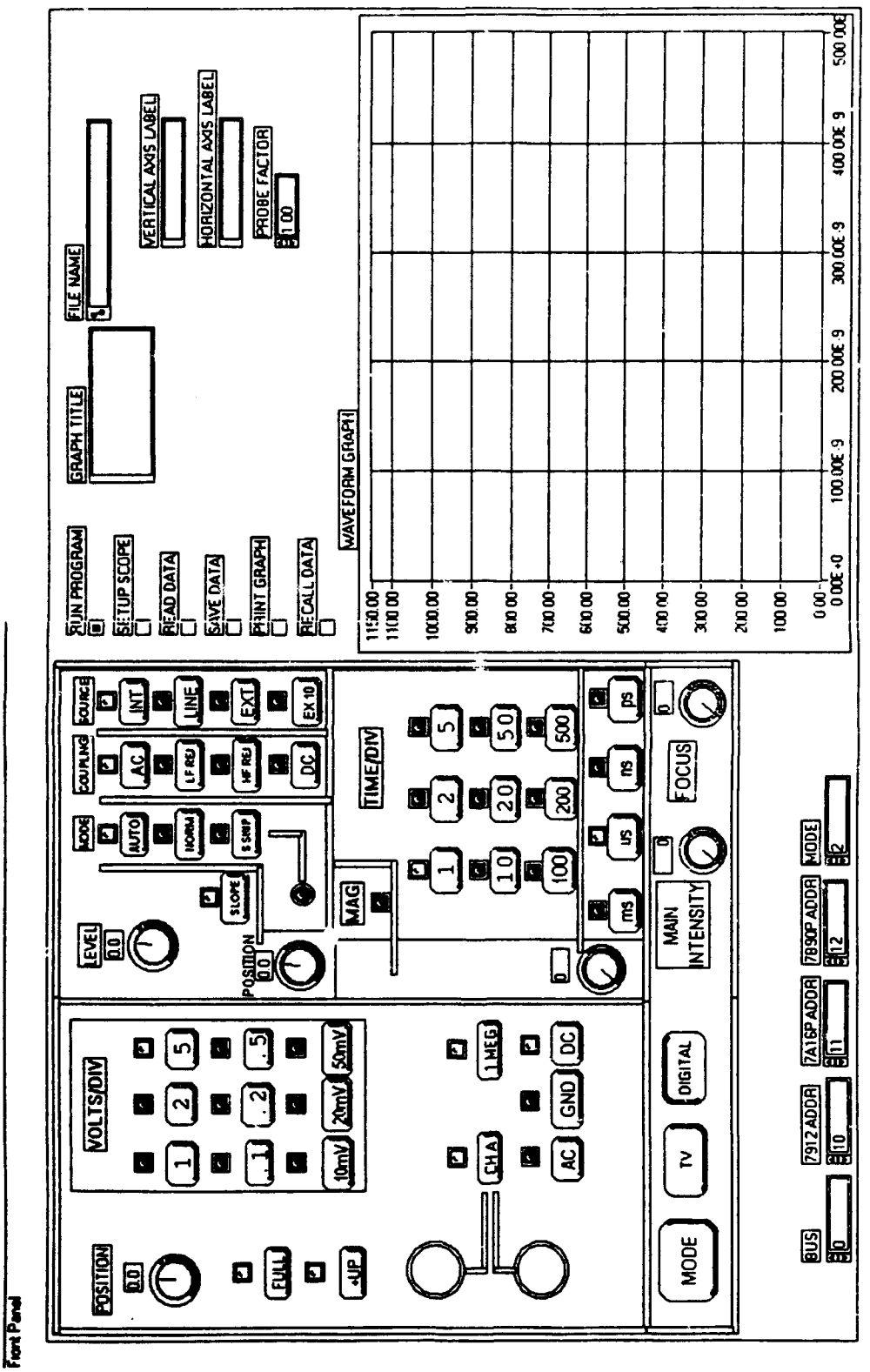

Figure A-1. Front panel for LabVIEW Tek7912 instrument driver.

No. of Copies	Organization
2	Administrator Defense Technical Info Center ATTN: DTIC-DDA Cameron Station (w/Form 50) Alexandria, VA 22304-6145
1	Director U.S. Army Research Laboratory ATTN: AMSRL-OP-AP-A Technical Publishing 2800 Powder Mill Road Adelphi, MD 20783-1197
1	Director U.S. Army Research Laboratory ATTN: AMSRL-OP-AP-AD Records Management 2800 Powder Mill Road Adelphi, MD 20783-1197
5	U.S. Army Research Laboratory ATTN: AMSRL-OP-AP-I (Tech Lib) Bldg. 305 APG-AA
1	Office of Director Defense Research & Engineering/Advanced Technology ATTN: ODDREAT (Dr. Dix) Rm 3D1089, The Pentagon Washington, DC 20310-3080
1	Office of Assistant to the Secretary of Defense (Atomic Energy) ATTN: ATSD(AE) (Dr. Harold Smith) Rm 3E1074, The Pentagon Washington, DC 20310
1	Ballistic Missile Defense Organization ATTN: DTD The Pentagon Washington DC 20301-7100
2	Dept of Army Asst Secy Army Research Dev Acqustn ATTN: SARD-DOV ATTN: SARD-ZT Rm 3E411, 103 Army Pentagon Washington DC 20310-0103

No. of Copies	Organization
1	Commander U.S. Army Materiel Command Deputy Chief of Staff for Research, Development, and Engineering 5001 Eisenhower Avenue Alexandria, VA 22333-0001
1	Commander U.S. Army Materiel Command ATTN: AMCAQ-M 5001 Eisenhower Avenue Alexandria, VA 22333-0001
1	Director U.S. Army Research Laboratory ATTN: AMSRL-D (Dr. Lyons) 2800 Powder Mill Road Adelphi, MD 20783-1145
1	Deputy Director U.S. Army Research Laboratory ATTN: AMSRL-DD (Dr. Frasier) 2800 Powder Mill Road Adelphi, MD 20783-1145
1	Director U.S. Army Research Laboratory Survivability/Lethality Analysis Directorate ATTN: AMSRL-SL (Dr. Wade) Aberdeen Proving Ground, MD 21005-5068
1	Director U.S. Army Research Laboratory Weapons Technology Directorate ATTN: AMSRL-WT (Dr. May) Aberdeen Proving Ground, MD 21005-5066
1	Director U.S. Army Research Laboratory Survivability/Lethality Analysis Directorate ATTN: AMSRL-SL-I (Dr. Starks) Aberdeen Proving Ground, MD 21005-5068
1	Director U.S. Army Research Laboratory Survivability/Lethality Analysis Directorate ATTN: AMSRL-SL-C (Mr. Hughes) Aberdeen Proving Ground, MD 21010-5423

No. of Copies	Organization
6	Director U.S. Army Research Laboratory Survivability/Lethality Analysis Directorate ATTN: AMSRL-SL-CS (Mr. Beilfuss) (1 cy) ATTN: AMSRL-SL-CS (Mr. B. Smith) (5 cys) Aberdeen Proving Ground, MD 21010-5423
1	Director U.S. Army Research Laboratory Survivability/Lethality Analysis Directorate ATTN: AMSRL-SL-E (Mr. Mares) White Sands Missile Range, NM 88002-5501
1	Director U.S. Army Research Laboratory Survivability/Lethality Analysis Directorate ATTN: AMSRL-SL-B, Bldg 328 (Dr. Deitz) Aberdeen Proving Ground, MD 21005-5068
4	U.S. Army Research Laboratory Nuclear & Directed Energy Div. ATTN: AMSRL-WT-N ATTN: AMSRL-WT-NA ATTN: AMSRL-WT-NB ATTN: AMSRL-WT-ND 2800 Powder Mill Rd Adelphi, MD 20783-1145
1	Director U.S. Army Research Laboratory Technology Transfer Office ATTN: AMSRL-TT 2800 Powder Mill Road Adelphi, MD 20783-1145
1	Director U.S. Army Research Laboratory Program and Budget Office ATTN: AMSRL-PB-P (Mr. Sczepanski) 2800 Powder Mill Road Adelphi, MD 20783-1145
2	Director U.S. Army Research Laboratory Electronics and Power Sources Directorate ATTN: AMSRL-EP (Dr. Thornton) ATTN: AMSRL-EP-M Fort Monmouth, NJ 07703-5601

No. of Copies	Organization
2	Technical Director U.S. Army Communications-Electronics Command, RD&E Center ATTN: AMSEL-RD ATTN: AMSEL-RD-AE Fort Monmouth, NJ 07703-5201
1	Commander U.S. Army Aviation and Troop Command Aviation Applied Technology Directorate ATTN: AMSAT-R-TV Fort Eustis, VA 23604-5577
3	Commander U.S. Army Test and Evaluation Command ATTN: AMSTE-CG ATTN: AMSTE-TA ATTN: AMSTE-TD Aberdeen Proving Ground, MD 21005-5055
1	Commander U.S. Army Test and Evaluation Command ATTN: STEWS-TE-RE White Sands Missile Range, NM 88002-5000
1	Commander U.S. Army Test and Evaluation Command Combat Systems Test Activity ATTN: STECS-CO, Bldg 400 Aberdeen Proving Ground, MD 21005
1	Commander White Sands Missile Range ATTN: STEWS-TE-RE White Sands Missile Range, NM 88002
2	Commander U.S. Army Training and Doctrine Command ATTN: ATCD-SB ATTN: ATCD-H Fort Monroe, VA 23651-5000
3	Defense Nuclear Agency ATTN: Deputy Director ATTN: SPSP ATTN: TAIC 6801 Telegraph Road Alexandria, VA 22310-3398

No. of Copies	Organization
2	Director U.S. Army Materiel System Analysis Activity Evaluation and Support ATTN: AMXSY-ST ATTN: AMXSY-R Aberdeen Proving Ground, MD 21005-5071
1	Space and Naval Warfare Sys Cmd SPAWAR 332 2451 Crystal Park 5 Arlington, VA 22245-5200
1	Naval Research Lab Superintendent, Plasma Physics Div. ATTN: Code 6700 4555 Overlook Ave SW Washington, DC 20375-5320
1	Office of Naval Research Code 31 800 N. Quincy St. Arlington, VA 22217-5660
1	Naval Research Laboratory Supt. Electronics Science & Tech Div. Code 6800 4555 Overlook Ave SW Washington, DC 20375-5320
1	Phillips Laboratory PL/WS Kirtland AFB NM 87117-6008
1	Wright Laboratory EW Division WL/AAW, Bldg 620 2241 Avionics Circle, Suite 16 Wright-Patterson AFB, OH 45433-7318
1	Phillips Laboratory Dir. of Lasers and Imaging PL/LI Kirtland AFB, NM 87117-5776

No. of Copies	Organization
1	Wright Laboratory Dir. of Electronic Tech WL/EL Wright-Patterson AFB, OH 45433-6543
1	Rome Laboratory Dir. of Electromagnetics RL/EE Hanscom AFB, MA 01731
	Program Executive Officer Standard Army Management Information Systems ATTN: SFAE-PS-P *(abstract only)* 9390 Hall Road, Suite 142 Ft. Belvoir, VA 22060-5526
	Commander U.S. Army Materiel Command ATTN: AMCAM-LG *(abstract only)* 5001 Eisenhower Avenue Alexandria, VA 22333-0001
	Director U.S. Army Concepts Analysis Agency Requirements Directorate ATTN: CSCA-TCA (Mr. Barrett) 8120 Woodmont Avenue *(abstract only)* Bethesda, MD 20814-2797